

# Photo-CIDNP MAS NMR beyond the $T_1$ limit by fast cycles of polarization extinction and polarization generation

Eugenio Daviso <sup>a</sup>, Anna Diller <sup>a</sup>, A. Alia <sup>a</sup>, Jörg Matysik <sup>a,\*</sup>, Gunnar Jeschke <sup>b</sup>

<sup>a</sup> *Leiden Institute of Chemistry, Einsteinweg 55, P.O. Box 9502, 2300 RA Leiden, The Netherlands*

<sup>b</sup> *Institut für Physikalische Chemie, Universität Konstanz, 78457 Konstanz, Germany*

Received 17 August 2007; revised 1 October 2007

Available online 9 October 2007

## Abstract

In nanosecond-laser flash photo-CIDNP MAS NMR, polarization generation (PG) proceeds much faster than longitudinal spin relaxation. With a nanosecond-laser setup linked to the NMR console the repetition time of the experiment is then limited by the minimum recycle delay of the NMR spectrometer and the maximum repetition rate of laser flashes. These limits can only be reached if polarization left after the NMR experiment is completely canceled before the next laser flash. We introduce a presaturation pulse sequence, based on three  $(\pi/2)$   $^{13}\text{C}$  pulses and optimized timing and phase cycling that allows for such efficient polarization extinction (PE). The technique is demonstrated on selectively isotope labeled bacterial reaction centers (RCs) of *Rhodobacter (Rb.) sphaeroides* wildtype (WT). High-quality  $^{13}\text{C}$  photo-CIDNP MAS NMR spectra are obtained using cycle rates up to 4 Hz. The PE–PG strategy proposed here provides a general experimental scheme for reduction of measurement time in magnetic resonance experiments based on fast PG.

© 2007 Elsevier Inc. All rights reserved.

**Keywords:** MAS NMR; Solid-state photo-CIDNP effect; Laser flash NMR; Polarization generation; Polarization extinction

## 1. Introduction

Magnetic resonance experiments are repeated to improve signal-to-noise ratio by data accumulation. In the usual case, transitions of the detected nucleus or of a nucleus serving as a polarization source for cross-polarization are saturated by an initial  $(\pi/2)$  pulse. The repetition frequency is then limited by the kinetics of equilibrium recovery of this nucleus (Fig. 1A). This signal recovery depends on nuclear spin relaxation processes, which can be described phenomenologically by the three Bloch equations [1]. In particular, the longitudinal relaxation time  $T_1$  characterizes the recovery of Boltzmann populations on a transition of a nuclear spin that interacts thermally with its surroundings. This kinetic parameter is a materials property and can be between milliseconds and several months [2]. For heavy nuclei such as  $^{13}\text{C}$  in a rigid environ-

ment, as in the solid state,  $T_1$  often is in the range of several seconds or minutes, providing a serious limit to the rate of signal accumulation.

Recent developments of methods for polarization generation (PG) improve the sensitivity of NMR by several orders of magnitude by creation of transient highly polarized non-Boltzmann nuclear spin states, often termed as hyperpolarized states (Fig. 1B). Examples for PG methods used in solid state are optical pumping [3], dynamic nuclear polarization (DNP) [4], optical nuclear polarization [5], and the solid-state photo-CIDNP effect [6,7]. In solids, photochemically induced dynamic nuclear polarization (photo-CIDNP) has been observed for the first time in quinone-blocked frozen samples of RCs of *Rb. sphaeroides* R26 under continuous illumination by magic angle spinning (MAS) solid-state NMR [8]. Until now, despite of plenty of efforts, the observation of the solid-state photo-CIDNP effect is limited to natural photosynthetic RCs. Using continuous illumination, photo-CIDNP has been observed by MAS NMR in purple non-sulfur bacterial

\* Corresponding author. Fax: +31 71 5274603.

E-mail address: [j.matysik@chem.leidenuniv.nl](mailto:j.matysik@chem.leidenuniv.nl) (J. Matysik).




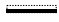

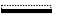
A	B	C
 49.99 %	 51.50 %	 50.00 %
 50.01 %	 48.50 %	 50.00 %
Boltzmann distribution	Hyperpolarized states	Polarization extinction

Fig. 1. Different regimes of population of the nuclear spin two-level system. (A) Boltzmann distribution for an ensemble of spins at thermal equilibrium. (B) Emissive hyperpolarization induced by the solid-state photo-CIDNP effect. (C) Saturation of the transition after polarization extinction (PE).

RCs from *Rhodobacter (Rb.) sphaeroides* wildtype (WT) and R26 [9,10], RCs from green sulfur bacterium *Chlorobium (C.) tepidum* [11], as well as in plant photosystems I and II [12–15]. Moreover, NMR signals were detected in entire membrane-bound photosynthetic units [16] and whole cells of *Rb. sphaeroides* [10]. Photo-CIDNP MAS NMR intensities are related to the local electron spin densities in the electron donor and the electron acceptor during the radical pair state. The origin of solid-state photo-CIDNP effect in photosynthetic RCs is explained by the parallel occurrence of up to three mechanisms [6,7,9,10]. The three-spin mixing (TSM) [17,18] depends on the coupling between two electron spins in a radical pair state, leading to enhanced electron polarization of the cofactors involved, which is transferred by anisotropic hyperfine (hf) coupling into polarization of nuclear spins. The differential decay (DD) mechanism [19] does not require electron–electron coupling if spin-correlated radical pairs have different lifetimes in their singlet and triplet states. In both mechanisms, high nuclear polarization is built up within hundreds of nanoseconds till microseconds by hyperfine interaction of the polarized electron pair with nuclei. The third mechanism is active in systems having a long-lived triplet state of the donor, which eventually leads to the differential relaxation (DR) between the nuclear spins in the triplet and in the singlet ground-state of the special pair [20,21]. In WT RCs, the DR mechanism does not occur since nuclear spin longitudinal relaxation is negligible since the triplet lifetime of the donor is short as 100 ns, while in R26 RCs a donor triplet lifetime of 100  $\mu$ s is sufficiently long to observe this effect. In photo-CIDNP MAS NMR, nuclear PG opens up additional polarization loss channels and therefore leads to enhanced signal recovery compared to longitudinal relaxation in the absence of PG [22].

Combination of the photo-CIDNP effect with selective isotope labeling allows for further increase of sensitivity and selectivity. Upon isotope labeling, natural spin diffusion spreads the nuclear polarization into the vicinity of the active cofactors. The effect is used in continuous illu-

mination experiments to map the electronic ground-state of the entire active cofactors as well as their surrounding amino acids of the protein [23–26]. On the other hand, spin diffusion leads to a redistribution of the primary polarization and obscures the primary photo-CIDNP MAS NMR intensities which provide information on electron spin densities. While such spin diffusion in photo-CIDNP MAS NMR experiments on selectively isotope labeled samples allows one to obtain chemical shift information of an area beyond the radical pair, it thus makes a reconstruction of the electron spin density distributions difficult. In contrast, laser flash photo-CIDNP MAS NMR experiments would allow both to obtain the true electron spin densities and to observe the ground-state information of the radical pair as well as its surroundings. Furthermore, the application of laser flashes enables time-resolved photo-CIDNP MAS NMR experiments. Hence, laser flash photo-CIDNP MAS NMR experiments allow for studying the mechanism that generates photo-CIDNP in great detail, while continuous illumination experiments show only a net effect and average information on the electronic structure of the radical pair state.

In order to perform such time-resolved experiments with a well-defined initial state of the spin system and with maximum possible repetition rate, any coherence and polarization still existing before the start of a new experiment needs to be extinguished. Otherwise residual polarization builds up during subsequent photocycles, as we recently discussed in some detail [22] and can be transferred by spin diffusion to nuclei that are not polarized in the primary event [Daviso et al., unpublished results]. The present paper is concerned with the technique of polarization extinction (PE) by equalizing the populations at the two levels of a nuclear spin transition before the PG event (Fig. 1C). As a consequence of such presaturation, the memory of the spin system is erased and the experiment detects only processes initiated by the next PG event. In the literature, a few cases of optimized PE, exclusively of  $^1\text{H}$  liquid-state NMR, have been reported [27–30], for example using WALTZ-16 for fast time-resolved liquid-state  $^1\text{H}$  photo-CIDNP studies [31]. Early DNP experiments on solids worked with add–subtract pulse sequences to eliminate effects of residual polarization [32]. Presaturation of  $^1\text{H}$  transitions by a train of an unspecified number of  $(\pi/2)$  pulses was employed in recent work on DNP supported by biradicals [33].

Here we present for the first time time-resolved laser flash photo-CIDNP MAS NMR data, which have been obtained by application of the proposed PE–PG strategy. This strategy combines optimized polarization extinction (PE) with polarization generation (PG) to allow for accumulation of time-resolved NMR data with repetition times much shorter than  $T_1$ . The new time limit on the repetition rate in such PE–PG experiments is given either by the minimum recycle delay of the NMR spectrometer or by the maximum repetition rate of the laser. The sig-

nificant speed-up of accumulation allows for more sensitive measurements on short-lived chemical states.

## 2. Materials and methods

### 2.1. Sample preparation

Cultures of *Rb. sphaeroides* WT (480 mL) were grown anaerobically in the presence of 1.0 mM [4-<sup>13</sup>C]-δ-aminolevulinic acid·HCl (ALA), which was purchased from Cambridge Isotope Laboratories (99% <sup>13</sup>C-enriched). The cultures were allowed to grow for 7 days in light. The culture was centrifuged for 10 min at 5500g and the combined pellet was resuspended in 40 mL 0.1 M phosphate buffer. The RCs were isolated as described by Shochat et al. [34]. A protein/pigment ratio  $A_{280}/A_{802} = 1.2$  was measured in the absorption spectrum to assess the purity of the samples. Approximately 15 mg of the labeled RC protein was used for the NMR experiments. For measurement of <sup>13</sup>C-isotope content, see [25].

### 2.2. MAS NMR measurements

The NMR experiments were performed on a DMX-200 NMR (Bruker-Biospin GmbH, Karlsruhe, Germany). All NMR spectra of histidine have been obtained at a temperature of 298 K and at a spinning frequency of 8 kHz. The spectra were collected with a Hahn echo pulse sequence with the CYCLOPS phase cycle of the ( $\pi/2$ ) pulse and detection under TPPM carbon–proton decoupling [35]. A total number of 512 scans per spectrum has been collected.

Photo-CIDNP spectra were obtained at a temperature of 243 K and at a spinning frequency of 8 kHz. The photo-CIDNP MAS NMR spectra were collected with a Hahn echo pulse sequence and two-pulse phase modulation proton decoupling. A total number of 67k scans per spectrum was collected. The optimum length of the ( $\pi/2$ ) carbon pulse, determined on uniformly <sup>13</sup>C-labeled histidine, varies from 4.8 to 5.0  $\mu$ s under our experimental conditions using a rf power of  $\sim 250$  W. The phases of the pulses in the PE–PG pulse sequences as shown in Figs. 3 and 7 are

$$\phi_1 = +x - x + x - x + x - x + x - x + x - x + x - x + x - x + x - x + x - x$$

$$\phi_2 = +x + x + y + y - x - x - y - y + x + x + y + y - x - x - y - y$$

$$\phi_3 = +y + y - x - x + y + y - x - x - y - y + x + x - y - y + x + x$$

$$\phi_4 = +x + x + y + y - x - x - y - y + x + x + y + y - x - x - y - y$$

## 3. Experimental

The setup for fast PE–PG experiments combines a nanosecond-flash laser setup with a modified MAS NMR spectrometer (Fig. 2).

### 3.1. Nanosecond-flash laser setup

A pulsed nanosecond-flash laser provides sufficient radiation intensity for time-resolved photo-CIDNP MAS NMR studies and does not decrease the time-resolution which can be obtained in NMR experiments. The laser is operating with a repetition rate between 1 and 10 Hz. Using 1064-nm flashes of a Nd:YAG laser (SpectraPhysics Quanta-Ray INDI 40-10, Irvine CA, USA), upon frequency-doubling with a second harmonic generator (SHG), 532-nm laser flashes with pulse length of 6–8 ns and an energy between 20 and 150 mJ are produced.

### 3.2. Electronic coupling of laser and NMR

The NMR console is used as master, while the laser is running in the mode of a slave. The connection is provided by a digital delay generator (DDG) (Model 9650A, Perkin-Elmer, Waltham, USA). The spectrometer generates the triggering impulse via a TTL channel for the DDG. The DDG triggers both pump lamp and Q-switch with a delay between 150 and 230  $\mu$ s in order to have optimum control of the energy output. The synchronization of the laser light pulse with the NMR rf pulse can be verified with a 500-MHz oscilloscope (Series TDS3000B, Tektronix, Beaverton, USA) connected to the output channel of the spectrometer as well as to a photodetector. The photodetector is consisting of a fast photodiode (FND-100, EG&G, Salem, USA) and a custom-made amplifier. The timing precision of the combined optical and NMR experiment has been demonstrated to be about  $\pm 1$  ns [7]. Note, however, that the time-resolution of photo-CIDNP experiments is limited by the length of the ( $\pi/2$ ) <sup>13</sup>C radio-frequency (rf) pulse used for NMR excitation. A typical value of this parameter is 5  $\mu$ s.

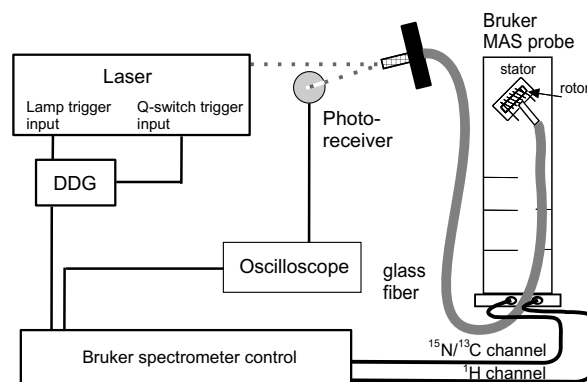


Fig. 2. Setup for nanosecond-laser flash photo-CIDNP MAS NMR.

### 3.3. Optical coupling of laser and NMR

Radiation emitted by the laser is transferred to the sample via a fiber bundle (FiberTech GmbH, Berlin, Germany). A multi-mode light fiber bundle provides high optical transparency in a broad spectral range as well as sufficient mechanical flexibility for being attached to the stator of the MAS probe. The optically active diameter is 3 mm and the numerical aperture is 0.22. The ratio of the radiation energies between input and output powers of the fiber bundle is 0.25. A Galilean lens system and a multi-mode fiber aligner are used for coupling the radiation pulses into the fiber bundle. The Galilean lens system, combining a concave lens with a convex one, allows collimation of the beam to the diameter required.

The MAS NMR probe head (DMX-200, Bruker-Biospin GmbH, Karlsruhe, Germany) has been modified in order to illuminate the rotor from the side [7,36]. This includes (a) a bore drilled into the most upper partition plate separating stator chamber and electronics, (b) drilling a small opening into the stator, and (c) winding a new coil from thin silver wire. The samples have been loaded into optically transparent sapphire MAS rotors to ensure homogeneous illumination.

## 4. Theory

### 4.1. General considerations

High time-resolution can be obtained by excitation of the electronic states with a nanosecond-laser flash. However, such experiments forfeit the advantage of a build-up of polarization during repeated photocycles that is inherent in experiments with continuous illumination. In recent work we have estimated that such build-up leads to further signal enhancement by a factor between 5 and 90 depending on the system under consideration [22]. This sensitivity loss of a time-resolved compared to a continuous experiment can at least partially be compensated by faster repetition, as the signal recovery in continuous illumination experiments is linked to  $T_1$  in the seconds to minutes range, while the signal in time-resolved experiments is generated on timescales between tens of nanoseconds and hundreds of microseconds. In practice, another limit may be imposed by the maximum technically feasible repetition rate of the laser and NMR pulses. However, this is still significantly faster than thermal equilibration of the spin system, in particular, since equilibration may also involve slow processes of polarization exchange with remote nuclei via spin diffusion.

A time-resolved experiment consists of PG by laser excitation, a variable evolution period, and NMR detection. After these steps, the nuclear spin system is generally in a not very well-defined non-equilibrium state. To start the next repetition of the experiment in a well-defined state, any remaining coherence and polarization have to be extinguished. Coherence decays with the transverse relaxation

time  $T_2$ , which in solids is on the timescale of milliseconds. As the detection period of an NMR experiment usually lasts until coherence has completely decayed and as the limit imposed by  $T_2$  on the permissible repetition rate is less stringent than the limits imposed by the maximum allowed duty cycle of the NMR spectrometer and maximum repetition rate of the laser, coherence is of no particular concern here. If coherence needs to be extinguished, the probe head should be fitted with a coil for supplying pulsed field gradients (PFG) along  $z$ . The phase of any coherence remaining after the experiment can then be scrambled by a single field gradient pulse [37].

However, as  $T_1$  in solids usually exceeds technical limits on the repetition time, residual nuclear polarization needs to be extinguished. For optimum performance, PE should be as complete as possible and should be achieved with a minimum number of pulses in a time that is sufficiently short to not impose another limit on the repetition rate. Minimization of the number of pulses is required to avoid excessive radiofrequency (rf) heating during fast repetition. Although in our current implementation, rf heating results almost exclusively from proton decoupling, use of new techniques for weak-power decoupling at high MAS speeds [38] would enhance the importance of power insertion by the presaturation sequence.

The presaturation sequence needs to be as short as possible, since polarization recovery by longitudinal relaxation and back transfer from remote nuclei, polarized via spin diffusion, compete with PE. Furthermore, sequence design has to consider imperfections in experimental setup as well as rf inhomogeneity, i.e., it should perform reasonably well for slight misadjustments of the flip angles of the presaturation pulses. Any phase cycling introduced in the presaturation sequence to suppress residual polarization must result in a constant detection phase. This is because the phase of the actual signal does not depend on settings in the presaturation sequence. In the following, we consider sequences of  $(\pi/2)$  pulses with such *additive* phase cycling and discuss how the other conditions can be met.

### 4.2. Residual polarization

After a single  $(\pi/2)$  pulse, some polarization remains as the flip angle has a small error  $\delta$ . This error may slightly vary with resonance offset  $\Omega$  as well as across the sample due to inhomogeneity of the rf field. If the polarization before the pulse is described by the density operator

$$\sigma_0 = pI_z, \quad (1)$$

the resulting density operator after a pulse with phase  $+x$  is given by

$$\sigma_1 = -p \cos \delta I_y + p \sin \delta I_z. \quad (2)$$

Polarization does not evolve during the periods of free evolution. Hence, neglecting for the moment any conversion of coherence back to polarization by later pulses, the residual polarization after  $n$  nominal  $(\pi/2)$  pulses is

$$p_1 = p \sin^n \delta. \quad (3)$$

Eq. (3) is valid for all signals, independently of their chemical shift or resonance offset  $\Omega$ , except for a possible slight variation of  $\delta$  with resonance offset. The required number  $n$  of pulses thus depends on the quality of PE needed and on the mean flip angle error  $\langle \delta \rangle$ .

The contribution to the residual polarization described by Eq. (3) cannot be canceled by phase cycling, as it does not depend on the phase of the first  $\pi/2$  pulse and only additive phase cycles are permissible. In contrast, the coherence created by the first pulse can be extinguished by additive phase cycling. The density operator after a first pulse with phase  $-x$  is given by

$$\sigma'_1 = p \cos \delta I_y + p \sin \delta I_z \quad (4)$$

so that a  $[(+x) + (-x)]$  cycle on this pulse leaves only the residual polarization term. Due to a slight deviation  $\Delta\phi$  in the relative phases of the  $+x$  and  $-x$  pulses from  $180^\circ$ , a small fraction  $p_2 = [2(1 - \cos \Delta\phi)]^{1/2} p \ll p$  of the coherence may survive such phase cycling. Alternatively, if a PFG setup is available, the coherence can be destroyed by a field gradient pulse.

A second pulse will reconvert part of the coherence (transverse magnetization) to polarization. To quantify this, we have to consider evolution and relaxation of the coherence during interpulse delay  $t_{ip}$  between the  $\pi/2$  pulses that we associate with time  $d_2$  in Fig. 3. Before the second pulse we find

$$\sigma_2 = -p_2 \exp(-t_{ip}/T_2) \cos \delta \cos(\Omega t_{ip}) I_y + p_2 \exp(-t_{ip}/T_2) \cos \delta \sin(\Omega t_{ip}) I_x + p \sin \delta I_z. \quad (5)$$

After this pulse the density operator is described by

$$\sigma_3 = p_2 \exp(-t_{ip}/T_2) \cos^2 \delta \sin(\Omega t_{ip}) I_z + p_2 \exp(-t_{ip}/T_2) \cos \delta \sin \delta \cos(\Omega t_{ip}) I_y + p_2 \exp(-t_{ip}/T_2) \cos \delta \sin(\Omega t_{ip}) I_x - p \sin \delta \cos \delta I_y + p \sin^2 \delta I_z. \quad (6)$$

Note that the last term on the right-hand side of Eq. (6) corresponds to the contribution described by Eq. (3) with  $n = 2$ . In Eq. (6),  $\sin(\Omega t_{ip})$  can have any value in the range between  $-1$  and  $1$ . Thus, the contribution to residual polarization from reconversion of coherence is given by

$$|p_3| \leq p_2 \exp(-t_{ip}/T_2) \cos^2 \delta, \quad (7)$$

with the actual magnitude depending on the resonance offset  $\Omega$ . This contribution can be minimized by prolonging  $t_{ip}$ . On the other hand, prolonging  $t_{ip}$  leads to some signal recovery by longitudinal relaxation. Assuming that  $p$  is an equilibrium polarization this creates an additional contribution

$$p_4 = p[1 - \exp(-t_{ip}/T_R)], \quad (8)$$

where the recovery time  $T_R$  equals  $T_1$  in the absence of illumination but can be shorter during continuous illumination for those signals that exhibit a photo-CIDNP effect. To optimize the sequence,  $t_{ip}$  needs to be adjusted so that the sum of  $p_3$  and  $p_4$  is minimized.

Usually one has  $T_R \gg T_2$  in solids. If  $t_{ip} \gg T_2$  and  $t_{ip} \ll T_R$  can be fulfilled simultaneously, both  $p_3$  and  $p_4$  are negligible with respect to  $p_1$ . In this situation the total residual polarization is well approximated by Eq. (3) for any number  $n$  of pulses. This is the situation that we meet in the experimental examples in this work.

If  $T_R$  and  $T_2$  are too close to each other to fulfil both these conditions, additional additive phase cycling has to be introduced. A phase cycle  $[(+x, +x) + (-x, +x) + (+x, -x) + (-x, -x)]$  applied to the two presaturation pulses eliminates contribution  $p_3$  except for a residual term  $p_5$  of the order  $2(1 - \cos \Delta\phi) \exp(-t_{ip}/T_2) p$ . The polarization after a two-pulse presaturation sequence is then given by

$$p_6 = p \sin^2 \delta + p_5. \quad (9)$$

Note that  $p_5$  is a signed quantity that depends on the resonance offset  $\Omega$ . For sequences with  $n$  pulses, complete additive phase cycling of all pulses ( $2^n$  steps) or field gradient pulses of sufficient amplitude and duration after each  $(\pi/2)$  pulse should be applied.

### 4.3. Relative phase of the pulses

Consider the pulse sequence  $(\pi/2)_{\phi_1} - t_{ip} - (\pi/2)_{\phi_2}$ . In a well resolved spectrum, the variance  $\sigma_\Omega$  of the resonance offset  $\Omega$  is much larger than the linewidth  $1/T_2$ . If  $t_{ip} > T_2$ , we thus have  $\Omega t_{ip} \gg 2\pi$  for typical  $\Omega$  values. Hence, after time  $t_{ip}$  has passed, the phase of the coherence for different nuclei is distributed over the whole possible range  $(0, 2\pi)$ . In a magnetization vector picture, transverse magnetization for the different nuclei is distributed over the whole  $xy$  plane. In this situation the relative phase of two consecutive pulses cannot be optimized for signal suppression throughout the whole spectrum.

If coherence reconversion is suppressed by complete additive phase cycling rather than by relaxation,  $t_{ip} \ll T_2$

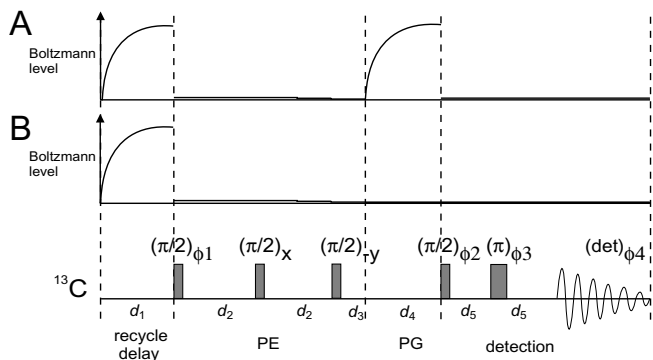


Fig. 3. Pulse sequence for a PE-PG experiment with longitudinal relaxation serving as the PG block. (A)  $d_1 = 12$  s,  $d_2 = 20$  ms,  $d_3 = 1$  ms,  $d_4 = 12$  s,  $d_5 = 125$   $\mu$ s (1/8000 Hz, i.e., MAS spinning rate),  $d_{\text{detection}} = 40$  ms. (B) as before, but with  $d_1 = 200$   $\mu$ s.

and hence  $t_{ip} \ll 1/\sigma_{\Omega}$  can be chosen. In this situation coherence reconversion by the second pulse in a pair of  $\pi/2$  pulses is further diminished if this pulse has a phase shift of  $\pm 90^\circ$  with respect to the first pulse. We implement this phase shift for the last two pulses in our presaturation sequence. Note that the  $90^\circ$  phase shift is compatible with additive phase cycling. The complete presaturation sequence is thus given by

$$(\pi/2)_{\phi_1} - t_{ip} - [(\pi/2)_{\phi_i} - t_{ip} - ]_{n-2} - (\pi/2)_{\phi_n} - T, \quad (10)$$

where time  $T$  between the last pulse of the presaturation sequence and the polarization generator should be kept as short as possible to prevent unnecessary polarization recovery. In this we assume that the polarization generator does not reconvert the small residual nuclear coherence to polarization. Phase  $\phi_1$  is generally cycled  $+x/-x$  with addition of both signals. For  $T_R \gg T_2$ , we use  $T_2 < 3t_{ip} \ll T_R$  and constant phases  $\phi_i = +x$  and  $\phi_n = -y$ . For  $T_R \approx T_2$ , each of the pulses in the square brackets in Eq. (10) should be phase cycled individually with  $\phi_i = +x/-x$  with addition of the signals and the last pulse should be cycled with  $\phi_n = -y/+y$  with addition of the signals. In this regime an odd number  $n$  of pulses gives better results than an even number, as the final reconversion of coherence to polarization is avoided. Unless  $t_{ip} \gg T_2$  can be chosen, an odd number of pulses is also advantageous in the regime  $T_R \gg T_2$ . The phase cycle of the presaturation sequence is combined with usual CYCLOPS phase cycling for the detection sequence.

## 5. Results and discussion

### 5.1. PE–PG experiments on histidine

The PE–PG pulse sequences are constructed of four building blocks: recycle delay, PE, PG and detection (Figs. 3 and 7). In both sequences, the PE is caused by a train of  $n = 3$  pulses with flip angle  $\pi/2$  of which only the first one is phase cycled  $[(+x) + (-x)]$ . Due to PE by presaturation, the recycle delay  $d_1$  is independent of  $T_1$  (or  $T_R$ ) and becomes limited by the minimum recycle delay of the NMR console, the necessity to avoid excessive rf heating by decoupling, or the maximum repetition rate of laser pulses. Experimentally, we found useful minimum values of about 200 ms corresponding to twice the limit imposed by the laser. In addition to phase cycling, we use an inter-pulse delay  $d_2$  of 20 ms, which is significantly longer than  $T_2$ , so that conversion of coherence to polarization can be neglected.

In the case of histidine, the PG is simply a relaxation delay  $d_4$  during which polarization recovery towards thermal equilibrium occurs. The two extreme cases for a Boltzmann spin system are shown in Traces A and B of Fig. 3. Long delays allow for complete signal recovery (Trace A), while for short delays the build-up of Boltzmann polarization is negligible (Trace B). Hence, experiments on histidine can be used for probing the efficiency of presaturation.

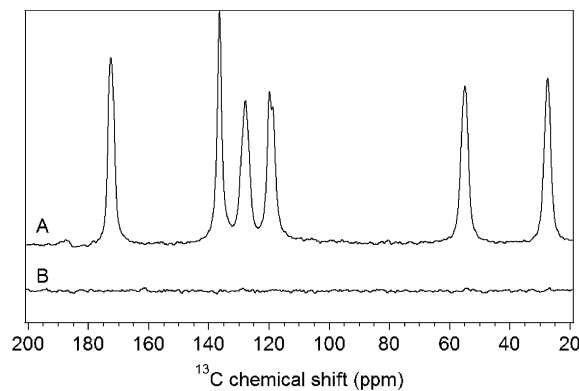


Fig. 4. Efficiency of polarization extinction (PE) for solid histidine. (A) Spectrum obtained according to Fig. 3A with a delay  $d_1 = d_4 = 12$  s. (B) Spectrum obtained according to Fig. 3B with a delay  $d_1 = 12$  s and  $d_4 = 200$   $\mu$ s.

Fig. 4 shows two spectra of uniformly  $^{13}\text{C}$ -labeled histidine. Both spectra have been measured using a Hahn echo pulse sequence with a recycle delay  $d_1$  of 12 s. In Spectrum 4A, the presaturation pulse sequence has been used with a relaxation delay  $d_4$  of 12 s, according to the polarization evolution shown in Trace 3A. A polarization evolution as shown in Trace 3B leads to Spectrum 4B, which has been collected with a short relaxation delay  $d_4$  of 200  $\mu$ s, corresponding to a total recovery time  $d_3 + d_4$  of 1.2 ms. Under these conditions, the signal is almost extinguished. Considering the magnitude spectra of both experiments, the ratio between the integrals of all signals  $B/A$  is  $< 0.25\%$ . For a longitudinal relaxation time of 10 s and a recovery time of 1.2 ms, only 0.012% of signal recovery would be expected. This indicates that the small residual signals are due to incomplete PE. However, a suppression of more than 99.75% of the initial polarization is certainly sufficient for fast PG solid-state NMR experiments, in which data are rarely accumulated to signal-to-noise ratios larger than 400.

The effect of the number of  $(\pi/2)$  PE pulses has been investigated in Fig. 5. Using three  $(\pi/2)$  PE pulses leads to the best results (Spectrum 5C). With  $n = 1$  and 2, significantly larger residual signals were observed (Spectra 5A and B), while  $n = 4$  did not lead to significant improvements with respect to  $n = 3$  (Spectrum 5D). Using three  $(\pi/2)$  PE pulses, the influence of  $d_2$  on PE is explored in Fig. 6. Short  $d_2$  values lead to imperfect PE (Spectra 6A and B), while a  $d_2$  of 20 ms is sufficiently long to allow for almost complete PE (Spectrum 6C). The data clearly demonstrate that  $d_2$  values longer than  $T_2$  are required to erase the signal, if only the first  $(\pi/2)$  pulse is phase cycled.

The residual signals observed with  $n = 1$  or 2 presaturation pulses are clearly out of phase, suggesting that they do not originate from a Hahn echo coherence transfer pathway. A complete 32-step phase cycle that combines  $[(+y) - (-x) + (-y) - (+x)]$  cycling on the  $\pi$  pulse with CYCLOPS on the  $\pi/2$  pulse of the echo subsequence and the additive phase cycling should cancel these signals and lead to improved performance.

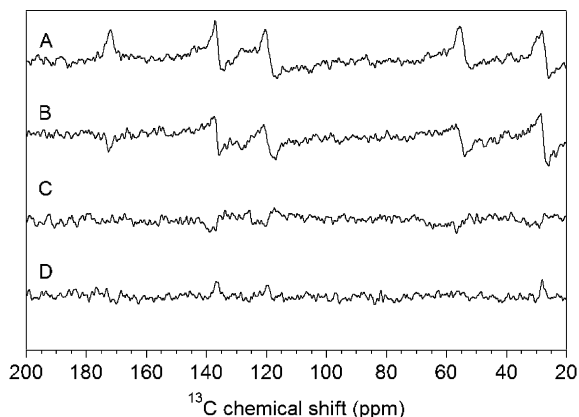


Fig. 5. Comparison of the efficiency of presaturation pulse sequences having one (A), two (B), three (C) and four (D)  $(\pi/2)$  pulses for solid histidine. For the presaturation pulse sequences with more than one  $(\pi/2)$ , the delay time  $d_2$  is 20 ms.

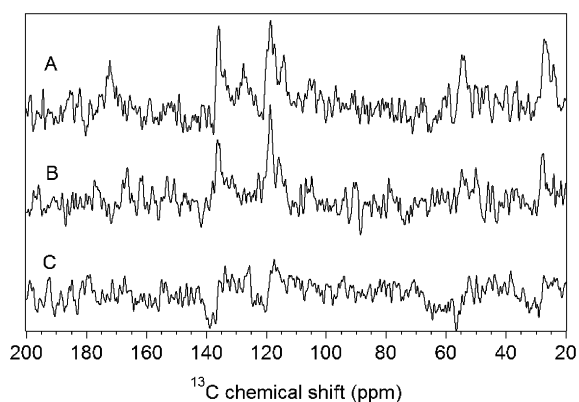


Fig. 6. Comparison of the efficiency of presaturation pulse sequences having three  $(\pi/2)$  pulses with different delay times  $d_2$  of (A) 5 ms, (B) 10 ms and (C) 20 ms. The sample is solid histidine.

### 5.2. Time-resolved $^{13}\text{C}$ PE–PG photo-CIDNP MAS NMR

In photo-CIDNP MAS NMR, PG occurs during a photocycle which is completed after a time of a few hundred nanoseconds to a few hundreds of microseconds, depending on the sample under consideration. Using a nanosecond-laser flash,  $d_4$  is not considered as relaxation delay but as the time delay between optical excitation and NMR detection (Fig. 7A). For capturing the earliest events,  $d_4$  should be as short as the hardware allows.

A strong solid-state photo-CIDNP effect has been observed with 4-ALA labeled WT RCs under continuous illumination under white light [23,25] leading to entirely negative signals [9]. In Fig. 8, a series of spectra from such a sample obtained with different  $d_4$  delays after the laser pulse is shown in Trace 8A. Already at a  $d_4$  delay of 2 ms (spectrum shown in red), strong signals appear exclusively in the aromatic region of the  $^{13}\text{C}$  NMR spectrum. This is in contrast to previous experiment under continuous illumination, in which also light-induced signals appear in the aliphatic region [23,25]. Data obtained at 60, 133 and 500 ms

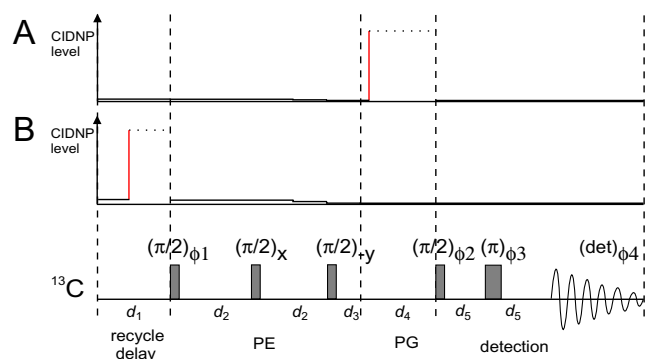


Fig. 7. Pulse sequence for a PE–PG experiment based on nanosecond-laser flash photo-CIDNP MAS NMR. (A) Laser flash during the polarization generation (PG) period. Values used for obtaining Trace 8A are:  $d_1 = 200$  ms,  $d_2 = 20$  ms,  $d_3 = 1$  ms,  $d_5 = 125$   $\mu\text{s}$  (1/8000 Hz, i.e., MAS spinning rate),  $d_{\text{detection}} = 30$  ms. Delay  $d_4$  is 2 ms (red), 60 ms (green), 133 ms (light blue) and 500 ms (dark blue). (B) Laser flash before the polarization extinction (PE) period. Values used for obtaining Spectrum 8C are as before, but  $d_4 = 500$  ms.

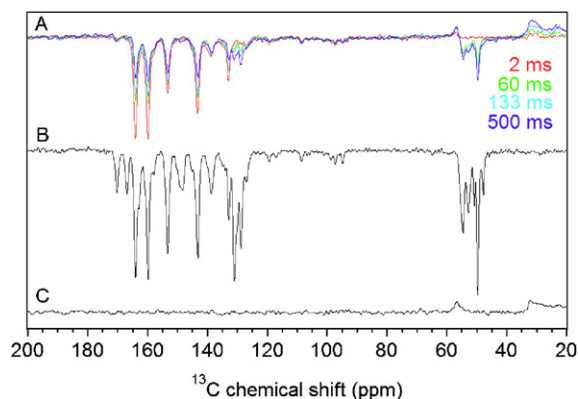


Fig. 8. Nanosecond-laser flash photo-CIDNP MAS NMR on *Rb. sphaeroides* WT photosynthetic reaction centers. (A) Superposition of spectra obtained with the sequence according to Fig. 7A and four different values of  $d_4$  being 2 ms (red), 60 ms (green), 133 ms (light blue) and 500 ms (dark blue). (B) Continuous illumination photo-CIDNP MAS NMR spectrum of *Rb. sphaeroides* WT photosynthetic reaction center. (C) Spectrum obtained with the sequence according to Fig. 7B.

(spectra shown in green, light blue and dark blue, respectively) show the exact kinetics of polarization transfer to the aliphatic carbons on the ms timescale which can be understood in terms of spin diffusion towards the steady-state envelope (Spectrum 8B). The differences between the laser flash experiment with a long delay  $d_4$  (dark blue spectrum in Trace 8A) and the steady state spectrum (Spectrum 8B) may be due to relaxation and further spin diffusion occurring under steady state conditions. The positive signals observed at the longer times can be assigned to the protein. They are not due to a solid-state photo-CIDNP effect but rather due to recovery of thermal polarization during the increasing  $d_4$  delay. These data demonstrate that with the PE–PG strategy nuclear polarization build-up and transfer can be observed with a time-resolution in the millisecond range.

For proving the efficiency of the PE in the photo-CIDNP MAS NMR experiment, the laser pulse is shifted before the presaturation into the  $d_1$  cycle delay (Trace 7B). Under these conditions, no significant solid-state photo-CIDNP effect appears (Spectrum 8C).

## 6. Conclusions and outlook

In traditional NMR, polarization is too valuable to consider polarization extinction (PE). Modern methods for fast and efficient polarization generation (PG), such as the solid-state photo-CIDNP effect, however, have a signal build-up independent of  $T_1$  and require fast-cycling PE–PG experiments for obtaining optimum sensitivity enhancement. PE is also required for time-resolved observation of polarization build-up in such experiments, as interference by polarization from previous photocycles has to be avoided. We have shown that the repetition rate can be dramatically reduced from 1 scan per 17 s, as required for optimum recovery of thermal equilibrium polarization, to about 4 scans per second. The new limit is imposed by restrictions of the hardware. We have further demonstrated that under these conditions, kinetic experiments with millisecond time-resolution are virtually undisturbed by residual polarization from previous photocycles. It appears reasonable to expect that polarization build-up and transfer can also be observed on the microsecond timescale. A similar PE–PG strategy may also be applicable to MRI, for instance in conjunction with the use of hyperpolarized gases in lung imaging or dissolved in the bloodstream, to safely assign observed contrast to a certain time after injection of the hyperpolarized contrast agent.

## Acknowledgments

E.D. thanks J. Disselhorst for help and suggestions for the construction of the laser setup. The authors thank Dr. P. Gast for help in sample preparation and exciting discussions. J.M. thanks Prof. H.J.M. de Groot for continuous support. This work has been financially supported by the Netherlands Organization for Scientific Research (NWO) through a Vidi Grant (700.53.423) to J.M. and an EMBO Grant (ASTF 131-2005) to E.D.

## Appendix A. Supplementary data

Supplementary data associated with this article can be found, in the online version, at [doi:10.1016/j.jmr.2007.10.001](https://doi.org/10.1016/j.jmr.2007.10.001).

## References

- [1] F. Bloch, Nuclear induction, *Phys. Rev.* 70 (1946) 460–474.
- [2] M. Levitt, *Spin Dynamics*, Wiley, Chichester, 2001.
- [3] D. Suter, J. Mlynek, Dynamics of atomic sublevel coherences during modulated optical-pumping, *Phys. Rev. A* 43 (1991) 6124–6134.
- [4] L.R. Becerra, G.J. Gerfen, R.J. Temkin, D.J. Singel, R.G. Griffin, Dynamic nuclear-polarization with a cyclotron-resonance maser at 5 T, *Phys. Rev. Lett.* 71 (1993) 3561–3564.
- [5] D. Stehlik, The mechanism of optical nuclear polarization in molecular crystals, habilitationsschrift, April 1975, Universität Heidelberg, in: E.C. Lim (Ed.), *Excited States*, vol. 3, Academic Press, New York, 1977, pp. 203–303.
- [6] G. Jeschke, J. Matysik, A reassessment of the origin of photochemically induced dynamic nuclear polarization effects in solids, *Chem. Phys.* 294 (2003) 239–255.
- [7] E. Daviso, G. Jeschke, J. Matysik, Photo CIDNP MAS NMR, in: T.J. Aartsma, J. Matysik (Eds.), *Biophysical Techniques in Photosynthesis II*, Springer, Dordrecht, 2008, pp. 385–399.
- [8] M.G. Zysmilich, A. McDermott, Photochemically induced dynamic nuclear-polarization in the solid-state  $^{15}\text{N}$  spectra of reaction centers from photosynthetic bacteria *Rhodobacter sphaeroides* R-26, *J. Am. Chem. Soc.* 116 (1994) 8362–8363.
- [9] S. Prakash, A. Alia, P. Gast, H.J.M. de Groot, G. Jeschke, J. Matysik, Magnetic field dependence of photo-CIDNP MAS NMR on photosynthetic reaction centers of *Rhodobacter sphaeroides* WT, *J. Am. Chem. Soc.* 127 (2005) 14290–14298.
- [10] S. Prakash, A. Alia, P. Gast, H.J.M. de Groot, J. Matysik, G. Jeschke, Photo-CIDNP MAS NMR in intact cells of *Rhodobacter sphaeroides* R26: molecular and atomic resolution at nanomolar concentration, *J. Am. Chem. Soc.* 128 (2006) 12794–12799.
- [11] E. Roy, A. Alia, P. Gast, H.J. van Gorkom, H.J.M. de Groot, G. Jeschke, J. Matysik, Photochemically induced dynamic nuclear polarization in the reaction center of the green sulphur bacterium *Chlorobium tepidum* observed by  $^{13}\text{C}$  MAS NMR, *Biochim. Biophys. Acta* 1767 (2007) 610–615.
- [12] J. Matysik, A. Alia, P. Gast, H.J. van Gorkom, A.J. Hoff, H.J.M. de Groot, Photochemically induced nuclear spin polarization in reaction centers of photosystem II observed by  $^{13}\text{C}$ -solid-state NMR reveals a strongly asymmetric electronic structure of the P680 $^{+}$  primary donor chlorophyll, *Proc. Natl. Acad. Sci. USA* 97 (2000) 9865–9870.
- [13] A. Alia, E. Roy, P. Gast, H.J. van Gorkom, H.J.M. de Groot, G. Jeschke, J. Matysik, Photochemically induced dynamic nuclear polarization in photosystem I of plants observed by  $^{13}\text{C}$  magic-angle spinning NMR, *J. Am. Chem. Soc.* 126 (2004) 12819–12826.
- [14] A. Diller, A. Alia, E. Roy, P. Gast, H.J. van Gorkom, J. Zaenen, H.J.M. de Groot, C. Glaubitz, J. Matysik, Photo-CIDNP solid-state NMR on photosystems I and II: what makes P680 special? *Photosynth. Res.* 84 (2005) 303–308.
- [15] A. Diller, E. Roy, P. Gast, H.J. van Gorkom, H.J.M. de Groot, C. Glaubitz, G. Jeschke, J. Matysik, A. Alia,  $^{15}\text{N}$  photochemically induced dynamic nuclear polarization magic-angle spinning NMR analysis of the electron donor of photosystem II, *Proc. Natl. Acad. Sci. USA* 104 (2007) 12767–12771.
- [16] S. Prakash, A. Alia, P. Gast, G. Jeschke, H.J.M. de Groot, J. Matysik, Photochemically induced dynamic nuclear polarisation in entire bacterial photosynthetic units observed by  $^{13}\text{C}$  magic-angle spinning NMR, *J. Mol. Struct.* 661 (2003) 625–633.
- [17] G. Jeschke, Electron–electron–nuclear three-spin mixing in spin-correlated radical pairs, *J. Chem. Phys.* 106 (1997) 10072–10086.
- [18] G. Jeschke, A new mechanism for chemically induced dynamic nuclear polarization in the solid state, *J. Am. Chem. Soc.* 120 (1998) 4425–4429.
- [19] T. Polenova, A.E. McDermott, A coherent mixing mechanism explains the photoinduced nuclear polarization in photosynthetic reaction centers, *J. Phys. Chem. B* 103 (1999) 535–548.
- [20] R.A. Goldstein, S.G. Boxer, Effects of nuclear-spin polarization on reaction dynamics in photosynthetic bacterial reaction centers, *Biophys. J.* 51 (1987) 937–946.
- [21] A. McDermott, M.G. Zysmilich, T. Polenova, Solid state NMR studies of photoinduced polarization in photosynthetic reaction centers: mechanism and simulations, *Solid State Nucl. Magn. Reson.* 11 (1998) 21–47.



- [22] A. Diller, S. Prakash, A. Alia, P. Gast, J. Matysik, G. Jeschke, Signals in solid-state photochemically induced dynamic nuclear polarization recover faster than with the longitudinal relaxation time, *J. Phys. Chem. B* (2007), online.
- [23] J. Matysik, E. Schulten, A. Alia, P. Gast, J. Raap, J. Lugtenburg, A.J. Hoff, H.J.M. de Groot, Photo-CIDNP  $^{13}\text{C}$  magic angle spinning NMR on bacterial reaction centres: exploring the electronic structure of the special pair and its surroundings, *Biol. Chem.* 382 (2001) 1271–1276.
- [24] S. Prakash, A. Alia, P. Gast, H.J.M. de Groot, G. Jeschke, J. Matysik,  $^{13}\text{C}$  shift map of the active cofactors in photosynthetic reaction centers of *Rhodobacter sphaeroides* revealed by photo-CIDNP MAS NMR, *Biochemistry* 46 (2007) 8953–8960.
- [25] E.A.M. Schulten, J. Matysik, A. Alia, S. Kiihne, J. Raap, J. Lugtenburg, P. Gast, A.J. Hoff, H.J.M. de Groot,  $^{13}\text{C}$  MAS NMR and photo-CIDNP reveal a pronounced asymmetry in the electronic ground state of the special pair of *Rhodobacter sphaeroides* reaction centers, *Biochemistry* 41 (2002) 8708–8717.
- [26] J. Matysik, A. Alia, P. Gast, J. Lugtenburg, A.J. Hoff, H.J.M. de Groot, Photochemically induced dynamic nuclear polarization in bacterial photosynthetic reaction centre observed by  $^{13}\text{C}$  solid-state NMR, in: S.R. Kiihne, H.J.M. de Groot (Eds.), *Prospective on Solid State NMR in Biology*, Kluwer Academic Publishers, Dordrecht, 2001, pp. 215–225.
- [27] I. Kuprov, M. Goez, P.A. Abbott, P.J. Hore, Design and performance of a microsecond time-resolved photo-chemically induced dynamic nuclear polarization add-on for a high-field nuclear magnetic resonance spectrometer, *Rev. Sci. Instrum.* 76 (2005) 0841031–0841037.
- [28] M. Goez, I. Kuprov, K.H. Mok, P.J. Hore, Novel pulse sequences for time-resolved photo-CIDNP, *Mol. Phys.* 104 (2006) 1675–1686.
- [29] G.L. Closs, R.J. Miller, Laser flash-photolysis with NMR detection—microsecond time-resolved CIDNP—separation of geminate and random-phase processes, *J. Am. Chem. Soc.* 101 (1979) 1639–1641.
- [30] K.H. Mok, P.J. Hore, Photo-CIDNP NMR methods for studying protein folding, *Methods* 34 (2004) 75–87.
- [31] O.B. Morozova, A.V. Yurkovskaya, R.Z. Sagdeev, K.H. Mok, P.J. Hore, Time-resolved CIDNP study of native-state bovine and human alpha-lactalbumins, *J. Phys. Chem. B* 108 (2004) 15355–15363.
- [32] M. Afeworki, S. Vega, J. Schaefer, Direct electron-to-carbon polarization transfer in homogeneously doped polycarbonates, *Macromolecules* 25 (1992) 4100–4105.
- [33] K.N. Hu, H.H. Yu, T.M. Swager, R.G. Griffin, Dynamic nuclear polarization with biradicals, *J. Am. Chem. Soc.* 126 (2004) 10844–10845.
- [34] S. Shochat, T. Arlt, C. Francke, P. Gast, P.I. Vannoort, S.C.M. Otte, H.P.M. Schelvis, S. Schmidt, E. Vijgenboom, J. Vrieze, W. Zinth, A.J. Hoff, Spectroscopic characterization of reaction centers of the (M)Y210W mutant of the photosynthetic bacterium *Rhodobacter sphaeroides*, *Photosynth. Res.* 40 (1994) 55–66.
- [35] A.E. Bennett, C.M. Rienstra, M. Auger, K. Lakshmi, R.G. Griffin, Heteronuclear decoupling in rotating solids, *J. Chem. Phys.* 103 (1995) 6951–6958.
- [36] J. Matysik, A. Alia, J.G. Hollander, T. Egorova-Zachernyuk, P. Gast, H.J.M. de Groot, A set-up to study photochemically induced dynamic nuclear polarization in photosynthetic reaction centres by solid-state NMR, *Indian J. Biochem. Biophys.* 37 (2000) 418–423.
- [37] W.E. Maas, A. Bielecki, M. Ziliox, F.H. Laukien, D.G. Cory, Magnetic field gradients in solid state magic angle spinning NMR, *J. Magn. Reson.* 141 (1999) 29–33.
- [38] M. Ernst, M.A. Meier, T. Tüherm, A. Samoson, B.H. Meier, Low-power high-resolution solid-state NMR of peptides and proteins, *J. Am. Chem. Soc.* 126 (2004) 4764–4765.